Dynamics of Rims and the Onset of Spinodal Dewetting at Liquid/Liquid Interfaces

Rachel A. Segalman and Peter F. Green*

Department of Chemical Engineering, Texas Materials Institute, The University of Texas at Austin, Austin, Texas 78712

Received July 31, 1998; Revised Manuscript Received November 10, 1998

ABSTRACT: Atomic force microscopy was used to investigate dewetting instabilities of liquid films from solid and liquid substrates in three limiting cases. We examined dewetting of a poly(styrene-*co*-acrylonitrile) (SAN) copolymer of viscosity η_T(SAN) from a solid substrate, SiO_x, and from a liquid polystyrene (PS) substrate whose viscosity $\eta_S(PS) \gg \eta_T$ (SAN). The third case involved the dewetting of PS liquid films from liquid SAN substrates of varying thickness, H_S. In this latter case, the viscosity of the top PS liquid layer $\eta_T(PS) \gg \eta_S(SAN)$, the viscosity of the SAN substrate layer. SAN films dewet SiO_x substrates by a spinodal process when they were of thickness $H < 300$ Å. For $H > 300$ Å the SAN films were stable. For the situations in which the substrates were liquid PS films, SAN films of thickness $H_T(SAN) < 1000$ Å dewet via a spinodal mechanism whereas SAN films of $H_T(SAN) > 1000$ Å dewet the PS substrates by a mechanism involving the nucleation of holes with outer rims and the subsequent growth of these holes. Two regimes of growth were identified: an early stage regime where the hole initially nucleates and a rim is yet to form and a later stage regime where the rim exists. In this later stage, the hole radii $R_{SAN} \sim t$ and the width of the rims $l_{SAN} \sim t^{1/2}$. The height of the rims, q_{SAN}, increased at a more rapid rate with time than the width of the rims and $l_{SAN} \gg q_{SAN}$. In the final situation examined, where the PS films dewet the liquid SAN substrates ($\eta_T(PS) \gg \eta_S(SAN)$) of varying thickness, we identified a transition from low-viscosity liquid substrate-like behavior to solid substrate-like behavior when the thickness of the SAN substrate layer became sufficiently thin. Finally, we discuss significant differences in the mechanisms by which holes grow when the substrate viscosity is liquidlike and when it is solidlike.

Introduction

Wetting and dewetting of a solid substrate by a liquid polymeric film has received much attention experimentally and theoretically in recent years.[1−6] This interest is due, in part, to a range of technological applications including coatings, paints, and adhesives. A very thin nonwetting liquid film of thickness H, less than a critical thickness H_C, on a substrate can become unstable and dewet the substrate. The dewetting process, driven by long-range forces, results in the spontaneous formation of numerous holes, creating a characteristic spinodal pattern.[3,7] Films of thickness $H > H_C$, yet thinner than an equilibrium thickness, H_{eqb}, determined by a balance of gravitational and capillary forces, may also be unstable.[3] They dewet the substrate by a process involving the nucleation and growth of discrete holes with outer rims, as depicted in Figure 1. These holes grow until the rims eventually impinge and subsequently decay into a pattern of droplets due to a Raleigh instability.[3−6] Thicker films, $H > H_{eqb}$, on the other hand, can be stable. It is also possible for films on wettable substrates to become unstable. This might occur when the film becomes extremely thin. In this case, the instability proceeds by a spinodal mechanism driven by long-range forces. Recently, Reiter at al. showed that thick PDMS films on a wettable substrate in air can become unstable when placed in a different medium, water.[8]

The case of a liquid film dewetting a liquid substrate has received limited attention.[9−14] The nature of the instability should depend strongly on characteristics of both the dewetting polymer and the liquid substrate, as recently discussed by Brochard-Wyart et al.[9] Two limiting regimes can be identified: (a) a so-called solid substrate regime where the viscosity of the substrate η_S is much larger than the viscosity, η_T, of the top film and (b) a so-called liquid substrate regime where $\eta_S < \eta_T$.

The solid substrate regime, henceforth described in this paper as the *high-viscosity solidlike substrate* regime, occurs when

$$\eta_S > \frac{\eta_T}{\theta} \tag{1}$$

where θ is the equilibrium contact angle that the film makes with the substrate. In this regime, the radius, R, of a hole in the film should grow at a constant velocity

$$v \propto \frac{\gamma_T \theta^3}{\eta_T} \tag{2}$$

and

$$R \propto t \tag{3}$$

where γ_T is the surface tension of the unstable film.

Brochard-Wyart recently examined a limiting case ($\eta_S \rightarrow \infty$) where she showed that the growth rate of the hole exhibited different time dependencies depending on the dimensions of R.[9] She predicts that when a hole initially forms, the rim is absent, and it only appears after the radius of the hole reaches a critical value of $R_C \approx (bH)^{1/2}$, where b is the hydrodynamic extrapolation length,

$$b = a\frac{N^3}{N_e^{\,2}} \tag{4}$$

10.1021/ma981208w CCC: $18.00
Published on Web 01/20/1999

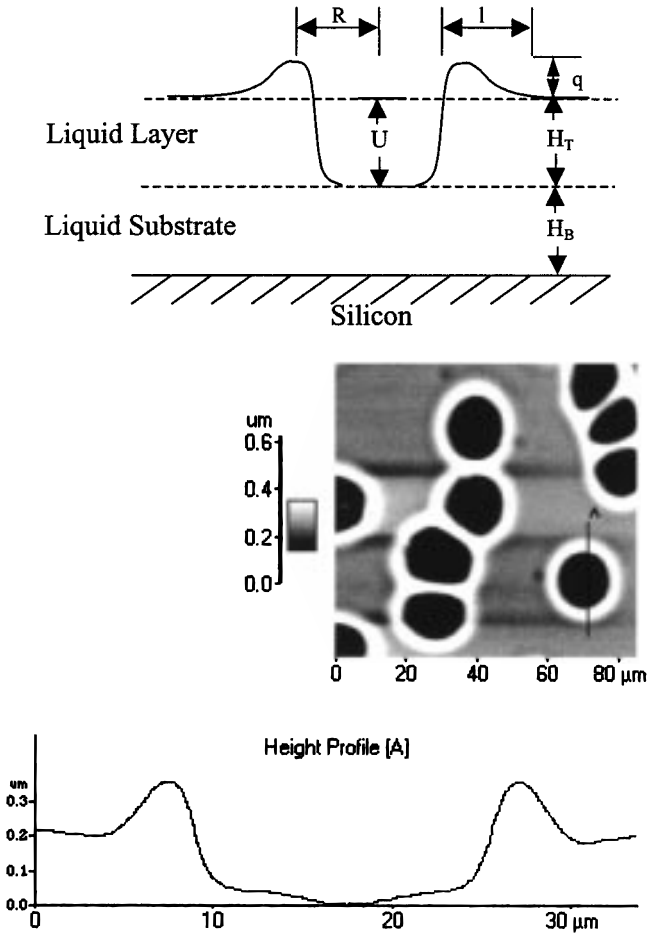

Figure 1. (a, top) Schematic of the growth of a hole in a thin-film bilayer. (b, bottom) Atomic force microscopy (AFM) 2-D image and cross-sectional line scan of a hole originating from nucleation and growth dewetting. This hole is typical of those found on solidlike substrates (H_T(SAN) > 1200 Å dewetting PS) after ~50 min of annealing.

In this equation, a is a monomer size, N is the degree of polymerization, and N_e is the number of monomers between entanglements. For small holes of $R < R_C = (bH)^{1/2}$, the rim is yet to form and R is predicted to increase exponentially. When $R_C < R < R_C'$ ($R_C' = b$), the rim is expected to have formed and R is expected to increase linearly with time. For $R > R_C'$ power law growth is expected.

A relationship between the width of the rim, $l(t)$, and the radius of the hole was determined assuming conservation of the volume. Here the shape of the hole is assumed to be cylindrical and that the material displaced to form the hole creates the outer rim.[8] Consequently,

$$l(t) \propto R^{1/2} \tag{5}$$

Equations 3 and 5 suggest that the width of the rim should be proportional to the square root of time:

$$l(t) \propto t^{1/2} \tag{6}$$

The liquid substrate regime, which we henceforth describe as the *low-viscosity substrate* regime ($\eta_S < \eta_T/\theta$), can be subdivided into three categories based on the ratio η_S/η_T: viscous, viscoinertial, and purely inertial. The viscous regime is characterized by the relative thickness of the substrate film, H_S, to the width of the rim, l. When $H_S > l(t)$, the velocity is constant. When $H_S < l(t)$, or polymer melt slippage takes place at the substrate surface, the hole radius grows with a power law dependence on time,[9]

$$R \propto t^{2/3} \tag{7}$$

and the velocity is

$$v = \theta_E^3 \left(\frac{\gamma_S}{\eta_S}\right)^{2/3} \left(\frac{H_S^2}{H_T}\right)^{1/3} \frac{1}{t^{1/3}} \tag{8}$$

In this case, the liquid−liquid interface is no longer constrained to a plane. The dewetting liquid layer is expected to deform to a characteristic lens-type shape,[9] penetrating the liquid substrate layer in the region of the rim, as illustrated in Figure 7, which will be discussed later.

Experimental observations of instabilities in thin liquid films at liquid/solid[3−6] and liquid/liquid[10−14] interfaces via nucleation and growth mechanisms have received much attention. However, spinodal dewetting at interfaces has received little attention,[7,11] primarily because its occurrence is uncommon. Thus far, no experimental studies have documented conditions under which the mechanism of the dewetting instability changes from nucleation and growth processes to spinodal dewetting processes, particularly at liquid/liquid interfaces.

Three basic issues are addressed in this paper.

1. We examine the dewetting of a liquid film of viscosity η_T from a wettable solid substrate and from a nonwettable high-viscosity, η_S, liquid substrate ($\eta_S \gg \eta_T$). In the former we show evidence of spinodal wetting when the liquid film is thinner than a critical thickness, H_C. In the latter we identify a critical film thickness, H_C', below which the mechanism by which the film dewets the substrate is by a spinodal process. Above H_C', dewetting occurs by nucleation and growth.

2. The situation in which a high-viscosity liquid film dewets low-viscosity liquid substrate layers ($\eta_T \gg \eta_S$) of varying thickness H_S is also addressed here. We show that when H_S becomes sufficiently small, the dewetting dynamics approaches that of the solid substrate-like condition.

3. We also show how the nucleation and growth mechanisms between dewetting from solidlike surfaces and low-viscosity surfaces differ.

Experimental Section

Bilayers of poly(styrene-*co*-acrylonitrile) (SAN) and polystyrene (PS) were prepared. Two situations were examined. In case I, a very high molecular weight PS was used as a bottom layer to create a situation where η_S(PS) ≫ η_T(SAN): the high-viscosity solidlike substrate case. We measured the viscosity of the SAN to be 2×10^6 P using a Rheometrics rheometer and the viscosity of PS, 2.6×10^9 P.[16] These thin-film bilayers were prepared by first spin-coating a toluene solution of PS onto the silicon. There was a thin layer of SiO_x, ~20 Å, determined by spectroscopic ellipsometry, on the silicon surface. A film of SAN in 4-methyl-2-pentanone was then spun onto a glass microscope slide. The edges of the slide were scored, and the film floated on a distilled water bath. The film was then recovered on top of the PS-covered wafer. This created a thin-film bilayer for which the substrate layer was several orders of magnitude higher in viscosity than the top. The final configuration of the sample is therefore vacuum/SAN/PS/SiO_x. All solutions were filtered before use.

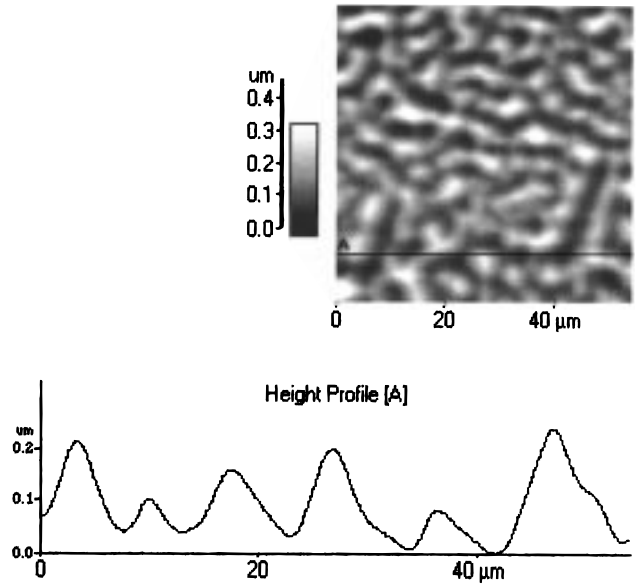

Figure 2. AFM 2-D image and cross-sectional line scan of the spinodal dewetting of H_T(SAN) ~ 1000 Å from PS after ~15 min of annealing.

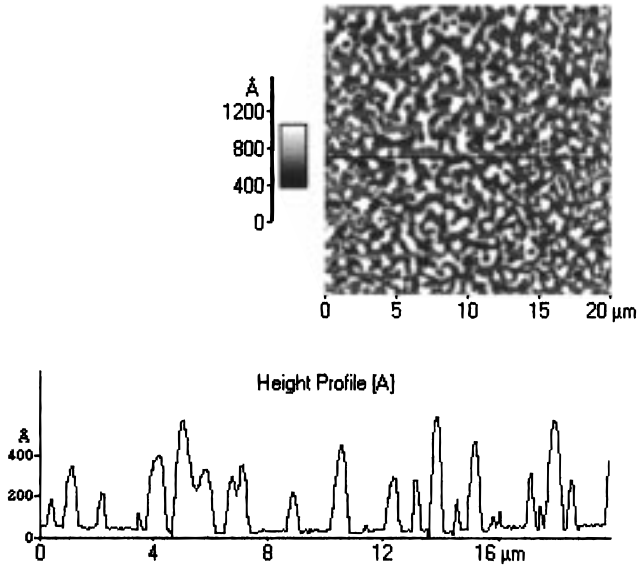

Figure 3. AFM 2-D image and cross-sectional line scan of the spinodal dewetting of H_T(SAN) ~ 200 Å from silicon after 3 h of annealing. The critical film thickness is H_{TC}(SAN) = 300 Å.

Case II refers to the opposite situation where η_S(SAN) ≪ η_T(PS): the low-viscosity liquid substrate case. In this situation, the films were prepared as described above, but with the positions of the films reversed (vacuum/PS/SAN/SiO_x). The characteristics of the polymers are as follows. The PS molecular weight was 1.6×10^6 with a dispersion index of 1.05, and the SAN molecular weight was 1.52×10^5 with a dispersion index of 1.97. The acrylonitrile content in this polymer was 25%. The thicknesses of the substrate films, H_S, were varied between ~1100 and 2400 Å by modifying the concentration of the solutions prior to casting. The top layer thickness, H_T, was held constant at ~1100 Å in all experiments.

After preparation, the films were characterized via ellipsometry and atomic force microscopy (AFM) with regard to thickness and film uniformity. The samples were dried and then annealed in a vacuum oven at 180 °C to initiate dewetting. They were removed from the oven and measured every few hours depending on dewetting velocity. We monitored the same hole in virtually every case. In some situations we monitored the behavior of a group of similar holes.

A Zeiss optical microscope was used to observe the long-range distribution and density of holes. A Park Scientific Autoprobe CP was operated in contact mode to examine the surface morphology of the samples. Line scans of at least five individual holes on each sample were determined at periodic intervals after annealing in a vacuum environment. Characteristics of the hole, its radius, R, its depth, U, the rim height, q, and the rim width, l, defined in Figure 1, were determined from the AFM line scans. The same area of the sample was investigated after each annealing step in order to follow the dynamics of the holes.

Results and Discussion

High-Viscosity Substrate Regime: Onset of Spinodal Dewetting (Case 1). As discussed earlier, this case refers to the situation in which the viscosity of the liquid substrate layer is significantly greater than that of the top SAN layer, η_S(PS) ≫ η_T(SAN). When the SAN layer thickness H_T(SAN) < H_{TC}(SAN) = 1000 Å, it became unstable by the spontaneous growth of small undulations creating a large number of holes reminiscent of a spinodal pattern (Figure 2). This is the result of capillary and long-range disturbances. These droplets, approximately 2000 Å in height with a characteristic width of 10 μm, are shown here. The wave vector obtained from a Fourier transform of the scan is $q = 0.13\ \mu m^{-1}$. This situation occurred after approximately 15 min of annealing. When films of thickness H_T(SAN) > 1000 Å are examined, the mechanism by which the SAN film dewets is by a nucleation and growth mechanism characterized by the formation and growth of discrete holes with rims (Figure 1b). The holes grow over time and eventually impinge, as discussed in detail later.

We also examined the interesting situation involving the stability of SAN on a wettable substrate, SiO_x. When H(SAN) < H_C ≈ 300 Å, the morphology of the unstable SAN film developed into a classic spinodal pattern (Figure 3) after several hours of annealing above T_g. This figure shows that the droplets are characterized by height ~500 Å and $q = 0.87\ \mu m^{-1}$. When H(SAN) > H_C(SAN), undulations in the surface are observed. These undulations dampen with anneal time. These films remain stable on the silicon beyond 1 week of annealing far above T_g.

A detailed study of the spinodal patterns is the subject of a forthcoming paper.[17] Below we concentrate on the details of the nucleation and growth process at liquid/liquid interfaces.

Dewetting of a Solidlike Substrate (η_S ≫ η_T) (Case I). Figure 1a shows a typical schematic of a bilayer sample in which a hole exists in the top layer. The relevant parameters, l, R, q, and U, which describe the characteristics of the hole, are shown here. An AFM image of holes in the SAN layer in a SAN/PS/SiO_x sample, together with a line scan showing the actual dimensions of a hole, is illustrated in Figure 1b. The rate at which the dimensions of this hole change with time is shown in Figure 4. The radius of the hole grows linearly with time, $R_{SAN} = 0.07t$, for t > 30 min. The first data point at t ≈ 15 min was obtained from a hole in its initial stages of formation and on which a rim was absent. As discussed earlier, in this regime where R < R_C, R increases exponentially with time. When $R_C' > R > R_C$, the growth is linear. The radius of this hole in its early stages of growth is approximately 2 μm. A rough calculation, using N = 1440, N_e(SAN) = 170, a = 3 Å, and H = 1250 Å, indicates that R_C ≈ 2 μm. We also

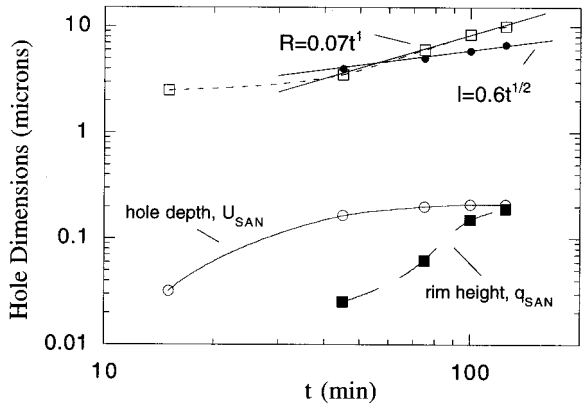

Figure 4. Characteristics of the dimensions of a hole in the top SAN layer (H_T(SAN) = 1200 Å) on PS (H_S(PS) = 2000 Å). The equations were obtained from least-squares fits to the data.

determined that $R_C' = b \approx 31\ \mu$m. Consequently, the latter data points are in the intermediate regime where linear growth is expected. We were unable to observe the late stage power law growth predicted by Brochard-Wyart because the holes impinged. Linear growth behavior has been observed by Lambooy et al.[10] and by Pan et al.[13] in other systems.

Information about the depth of this hole is relevant. It is clear from this figure that the hole continues to increase in depth while the rim forms. The width of this rim increases with the square root of time, $l = 0.6t^{0.5}$ (Figure 4). As discussed earlier, this prediction is based on a volume conservation argument. It turns out that an implicit assumption in the calculation is that the depth of the hole, U, of depth H_T.[9] So

$$l(t) \propto (RH_T)^{1/2} \tag{9}$$

Our data are consistent with this prediction when the conditions of the assumption are met, $t > 30$ min.

Since the dynamics of hole growth in this system are similar to the case of PS dewetting a solid substrate, it is constructive to compare the morphologies of the late stage growth in both situations. A noteworthy difference between the case of a solid substrate and an ultrahigh-viscosity substrate case, studied in this paper, is that upon reaching H_T a small dimple is excavated in the substrate before the hole depth stabilizes. Sharma and Reiter[4] observed the growth of uniform, circular, holes in PS on silicon. As demonstrated in Figure 1b, our holes are characterized by a shallow dimple in liquid substrate in the center of each hole. In both situations, the structures eventually coalesce into polygonal cellular structures as the holes impinged, as demonstrated in Figure 5a. In the solid substrate case, the polymer ribbons forming the polygonal edges then decayed into droplets neatly arranged in a polygonal pattern. Figure 5b demonstrates that, in the liquid−liquid case, the droplets did not assume this characteristic pattern. Instead, they appear randomly distributed on the surface of the film.

Low-Viscosity Substrate ($\eta_T \gg \eta_B$) (Case II). Below we examine the situation in which the top liquid layer has a much higher viscosity than the substrate layer. Varying thicknesses, H_S(SAN), of the substrate layer are investigated. As described in eq 7, the radius, R, of a hole in a liquid layer dewetting a lower viscosity liquid layer should grow as $t^{2/3}$. The data in Figure 6a for the

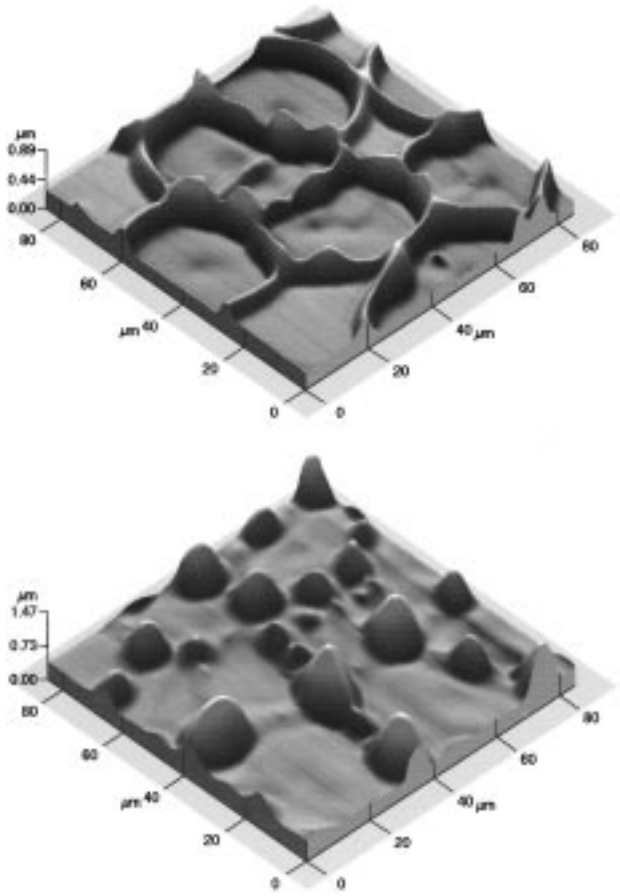

Figure 5. AFM perspective images of holes in H_T(SAN) ∼ 1500 Å on H_S ∼ 2000 Å showing the progression of hole growth to impinging cellular structures to droplets after annealing for (a, top) 200 min and (b, bottom) 500 min.

case in which H_S(SAN) = 2400 Å are consistent with $R_{PS} \sim t^{2/3}$. Qu et al.[14] observed power law growth with an exponent of $^2/_3$ in the PS/PMMA system when the viscosity of the PMMA substrate was low in comparison to the PS top layer thickness.

Let us now examine further details of the hole dynamics. Figure 7 illustrates the point that the hole depth is not limited to the depth of the unperturbed top film, H_T(PS). Rather, it excavates well into the substrate film. Figure 7a is a line scan of the bilayer after annealing. The rims are significantly broader and shorter than those observed in Figure 1b for the solid substrate case. Figure 7b is the same sample after the top film, PS, has been selectively dissolved using cyclohexane. Figure 7c is a schematic of the combination of these two line scans. At the liquid−liquid interface, a depression exists in the substrate in the region of the hole. This depression was not seen to extend more than 0.08 μm into the substrate layer, indicating that the substrate layer was not dewetting but merely being excavated due to forces translating from the top layer (Figure 7d). Around this depression, a ring is apparent in the liquid SAN. This ring is similar to a rim in the bottom surface of the dewetting film. This is characteristic of the lens-type shape expected in liquid−liquid dewetting, as discussed by Brochard-Wyart.[9] The presence of two rims, however, indicates that in this case not all of the material removed from the hole is stored in the rim visible from the top surface. As discussed below, this has important consequences regarding the growth rate of l. Both Lambooy et al. and Qu et al.

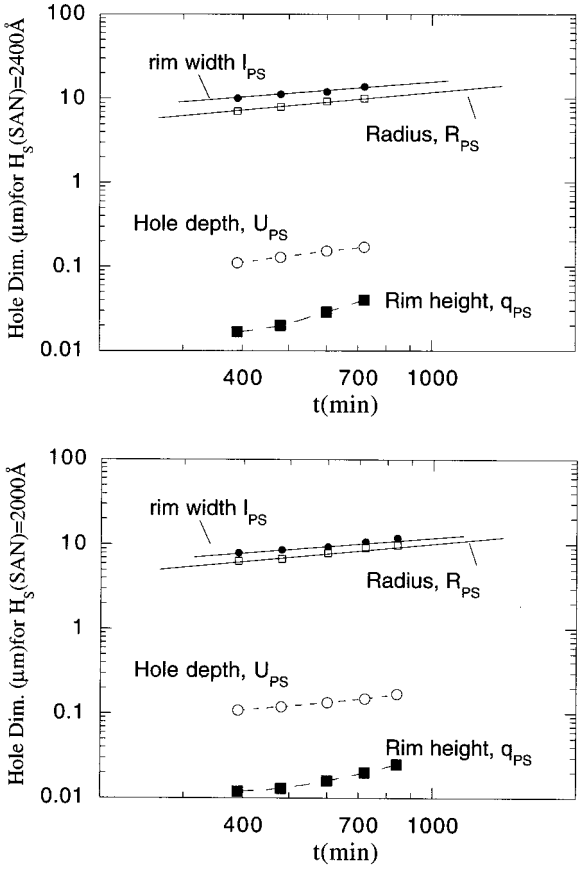

Figure 6. (a, top) Characteristics of the hole dimensions for a hole in a PS layer of thickness 1200 Å on a SAN film of thickness 2400 Å. The line through the rim width data has a power law dependence of $t^{1/2}$, and for R it is $t^{2/3}$. (b, bottom) A similar plot where the SAN bottom layer is H_S(SAN) = 2000 Å.

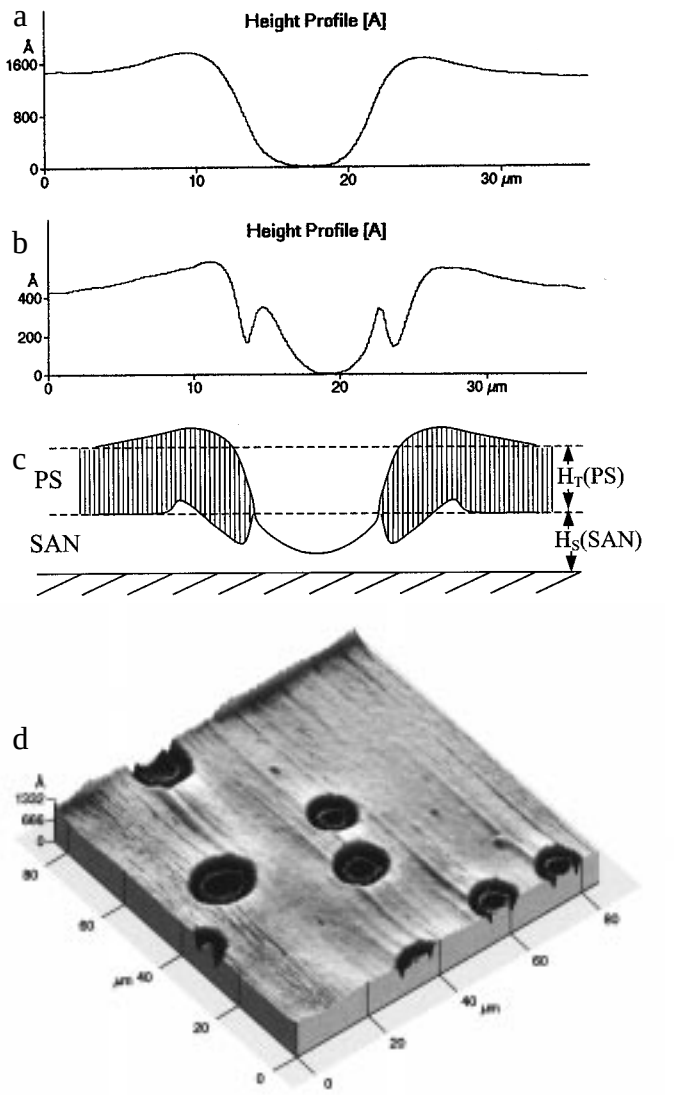

Figure 7. Hole morphology for liquidlike substrates. (a) An AFM line scan of the top surface of the bilayer after annealing. (b) An AFM line scan of the same hole after the top PS layer has been selectively removed. Note that while the X axes in (a) and (b) are the same, the Y axes are different. (c) A schematic of a hole dewetting from a liquid substrate. (d) A 3-D rendition of the bottom layer is shown here after the top layer was selectively dissolved.

reported depressions in the PMMA in the vicinity of the PS rim, after the PS top layer had been removed. In this case, the PS rim penetrated the PMMA layer, assuming the expected lens shape.

Unlike the case involving the solid substrate, the hole depth continued to increase throughout the experiment while R increased. We find that the width of the rim increased as t^k, where k varied between 0.5 and 0.6. That the exponent differs from 0.5 is not surprising considering the appreciable differences in the profile dynamics. Other noteworthy differences include the fact that $l > R$ in this case whereas Brochard-Wyart stipulated that $R > l$ in order to recover the $t^{1/2}$.

We might further compare the dynamics of rims for the solidlike substrate and liquid substrate cases. For both situations, the growth rate of the rim height $dq(t)/dt > dl(t)/dt$. For $\eta_S \gg \eta_T$ (SAN dewetting PS) the magnitude of the rim height, q_{SAN}, is larger than that of q_{PS} (PS dewetting the low-viscosity SAN substrate); moreover, $dq_{SAN}(t)/dt_s > dq_{PS}(t)/dt$. These differences could be a combination of the deformation of the SAN layer and the lower relative contribution of slip to shape of the rim in this soft substrate case. Similar observations were also made for the case where the SAN layer thickness was 2000 Å.

On a solid, nondeformable substrate, the velocity of a liquid spreading on the substrate, or a hole dewetting the substrate, is controlled by the viscosity of the liquid. However, the dynamics are expected to be much slower when the substrate is a liquid of similar surface tension because of the deformation of this underlying liquid layer. This was first discussed by Carre and Shanahan and by Shanahan in light of their experiments on the spreading of liquids.[18−20] They showed that a vertical force, due to capillarity, acting at the contact line is responsible for the deformation of the liquid substrate. As discussed by Long et al.,[21] the surface tension and the elasticity of the underlying liquid substrate deformation contribute to the change in free energy. This deformation induces flow inside the brush, leading to viscous dissipation. It should also affect the shape of the rims. We also observe the expected slowing down of the hole velocity for PS films dewetting SAN.

It is noteworthy that in the case of SAN dewetting PS (η_0(SAN) = 2 × 10^6 P and η_0(SAN) ≈ $10^3\eta_0$(PS)), we observed a constant hole velocity. Because of the large difference in the viscosity of the liquid PS substrate, the deformation, while expected, should be much smaller than that encountered for the dewetting of PS from SAN. Consequently, this deformation may not be large enough to have an immediate effect on the hole velocity

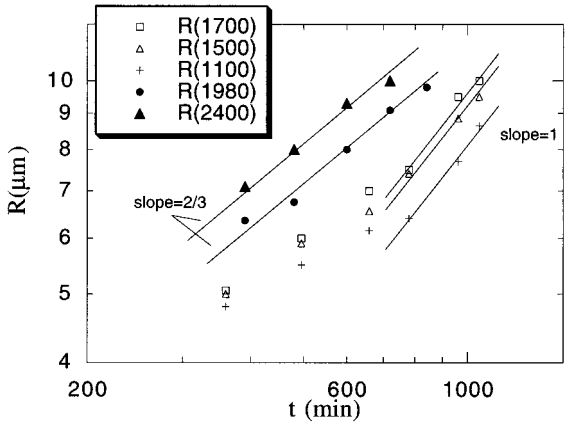

Figure 8. Growth of radii of holes in the top PS layer for SAN substrate layers of varying thickness.

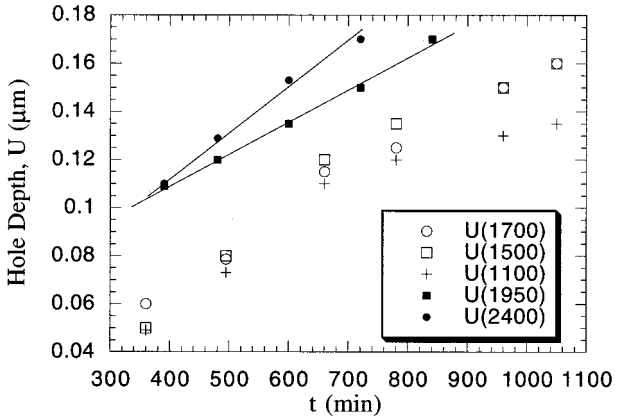

Figure 9. Dependence of hole depth, U, on time for varying SAN thickness. The lines are guides to the eye.

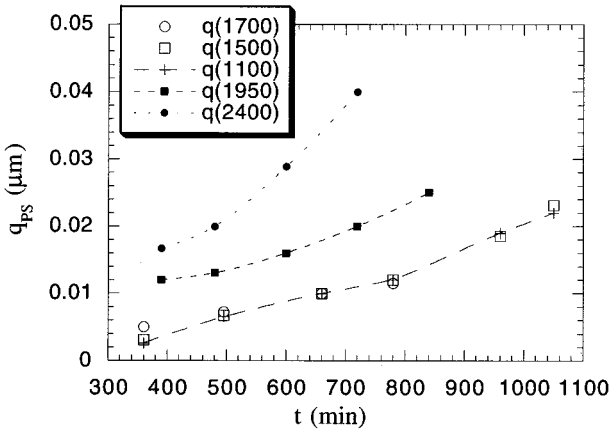

Figure 10. Plot of rim height vs time for PS dewetting from SAN substrates of varying thickness.

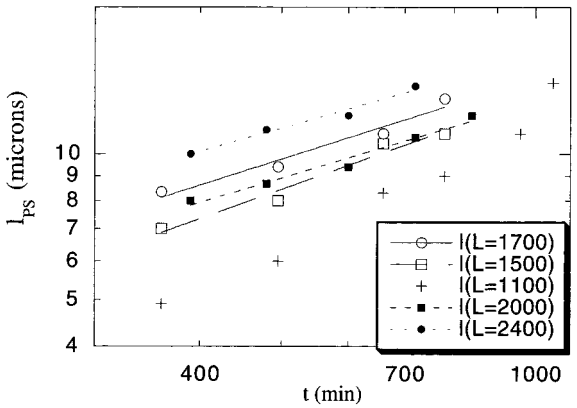

Figure 11. Plot of rim width vs time for PS dewetting from SAN substrates of varying thickness. The growth exponents for films of H_S(SAN) = 2400, 2000, 1700, and 1500 Å range between 0.5 and 0.6.

for SAN dewetting PS. The differences in the shape of the holes of the top layer of PS (Figure 1b) and of SAN (Figure 7a) are noteworthy. For SAN dewetting PS, a dimple is observed at the bottom of the hole, whereas the PS holes, for PS dewetting SAN, show no such undulations. In addition, the rim width to rim height ratios were much larger for SAN dewetting PS than for PS dewetting SAN. This should be related to the extent of the dissipation in the underlying liquid layer. Clearly, there are significant differences in the morphology of the holes depending on the viscosity of the liquid substrate and that of the overlying liquid film.

Solid Substrate-Mediated Effect. When the SAN layer thickness, H_S(SAN), is less than 2000 Å, the growth of the hole can no longer be described with a $t^{2/3}$ dependence. In fact, at long times, the data can reasonably be described by $R \sim t$, as shown in Figure 8, which shows the dependence of R on t for the SAN liquid substrate layers. Here it is clear that the growth rate increases when the radius reaches a size of approximately 6 μm, after 600 min.

It is instructive to consider the other characteristics of the hole. The hole depth (Figure 9) grows at a constant rate for the thicker SAN layer films, H_S(SAN) > 1700 Å. However, it appears to slow down considerably after 600 min, when the hole depth $U > 0.12$ μm. It is noteworthy that the rate of decrease of the velocity of U increases with decreasing SAN thickness; i.e., for $t > 600$ min, $dU/dt \sim 1/H_S$(SAN). The increase in the growth exponent of R to a value of 1 and the sudden decrease in the growth of the hole is consistent with the dynamics of a hole on a solidlike (or high viscosity) substrate.

An analysis of the time dependence and magnitude of q_{PS} (Figure 10) reveals that values of q_{PS} are virtually identical for the SAN films of H_S(SAN) < 2000 Å. However, the growth of the rim widths for all the SAN films, with the exception of the H_S(SAN) = 1100 Å layer, had growth exponents between 0.5 and 0.6 (Figure 11). The thin SAN film had shorter rim widths than the thick SAN layers, which is expected since dU_{PS}/dt approaches a constant value at long times.

It should be noted that in all cases the hole had not completely excavated to the silicon substrate. It is most probable that as the SiO_x substrate is approached, the effective viscosity of the liquid SAN increases. The decrease in dU/dt with decreasing SAN film thickness is consistent with this. The behavior described here corresponds to a transition from low-viscosity substrate behavior to the solidlike substrate case.

Concluding Remarks

We examined two limiting conditions of liquid/liquid dewetting. In one case we examined the dewetting of liquid SAN films from liquid PS layers in contact with solid silicon surfaces. We showed that when the thickness of the SAN layer was H_T(SAN) < 1000 Å, the film became unstable and dewetted the PS layer by a spinodal mechanism. Spinodal dewetting also accounted for the instability of SAN layers of thickness $H < 300$ Å on silicon substrates. When $H > 300$ Å, the SAN

layers remained stable. These results document the occurrence of spinodal dewetting on nonwettable and wettable substrates, respectively.

For the high-viscosity PS substrates, the instability proceeded by a nucleation and growth mechanism when the SAN layer thickness $H > 1000$ Å. This is reminiscent of the case of a liquid film dewetting a solid substrate, with some subtle differences. We identified two regimes of growth of the holes, an early stage regime and an intermediate stage regime, $(bH_S)^{1/2} < R < b$, where R increased linearly with time. This early stage regime corresponded to the growth of the hole before the rim formed.

This situation involving the dewetting of the high-viscosity PS film from SAN films of different thickness was somewhat different. When the SAN films were sufficiently thick, $H_{SAN} > 1700$ Å, the behavior was similar to that of a liquid film dewetting a low-viscosity liquid, with some notable exceptions. When $H_{SAN} < 1700$ Å, we observed a transition in the behavior reminiscent of the dewetting of a liquid film from a liquid substrate to dewetting from a solid substrate.

Acknowledgment. This work was supported by the National Science Foundation, DMR-9705101.

References and Notes

(1) Krausch, G. *J. Phys.: Condens. Matter* **1997**, *57*, 7741.
(2) Cazabat, A. M.; Heslot, F.; Levinson, P. In *Thin Films*; Ivanov, I. B., Eds.; Marcel Dekker: New York, 1987; pp 171−183.
(3) Brochard-Wyart, F.; Dalliant, J.*Can. J. Phys.* **1990**, *68*, 1084.
(4) Reiter, G. *Phys. Rev. Lett.* **1992**, *68*, 75.
(5) Sharma, A.; Reiter, G. *J. Colloid Interface. Sci.* **1996**, *178*, 383.
(6) Reiter, G. *Langmuir* **1993**, *9*, 1344.
(7) Bischoff, J.; Scherer, D.; Herminghaus, S.; Leiderer, P. *Phys. Rev. Lett.* **1996**, *77*, 1536.
(8) Reiter, G.; Casoli, A.; David, M.; Sharma, A.; Khanna, R.; Auroy, P., to be published.
(9) Brochard-Wyart, F.; Martin, P.; Redon, C. *Langmuir* **1993**, *9*, 3682. Brochard-Wyart, F.; Debregeas, G.; Fondecave, R.; Martin, P. *Macromolecules* **1997**, *30*, 1211.
(10) Lambooy, P.; Phelan, K. C.; Haugg, O.; Krausch, G. *Phys. Rev. Lett.* **1996**, *76*, 1110.
(11) Faldi, A.; Winey, K. I.; Composto, R. J. *Mater. Res. Soc. Symp. Proc.* **1995**, *366*, 71.
(12) Faldi, A.; Composto, R.; Winey, K. *Langmuir* **1995**, *11*, 4855.
(13) Pan, Q.; Winey, K.; Hu, H.; Composto, R. *Langmuir* **1997**, *13*, 1758.
(14) Qu, S.; Clarke, C. J.; Liu, Y.; Rafailovich, M. H.; Sokolov, J.; Phelan, K. C.; Krausch, G. *Macromolecules* **1997**, *30*, 3640.
(15) Milchev, A.; Binder, K. *J. Chem. Phys.* **1997**, *106*, 1978. Zhao, W.; Rafailovich, M.; Sokolov, J.; Fetters, L.; Plano, R.; Sanyal, M.; Sinha, S.; Sauer, B. *Phys. Rev. Lett.* **1993**, *70*, 1453.
(16) Graessley, W. W.; Roovers, J. *Macromolecules* **1979**, *12*, 959.
(17) Masson, J.-L.; Green, P. F. Manuscript in preparation.
(18) Shanahan, M. E. R. *Langmuir* **1995**, *11*, 1041.
(19) Shanahan, M. E. R.; Carre, A. *Langnuir* **1995**, *11*, 1396; Shanahan, M. E. R.; Carre, A. *Langnuir* **1994**, *10*, 1647.
(20) Shanahan, M. E. R. *J. Phys. D: Appl. Phys.* **1988**, *21*, 981.
(21) Long, D.; Ajdari, A.; Leibler, L. *Langmuir* **1996**, *12*, 1675.

MA981208W